THE JOURNAL OF PHYSICAL CHEMISTRY C
A JOURNAL OF THE AMERICAN CHEMICAL SOCIETY

pubs.acs.org/JPCC

Article

High-Pressure Behavior of δ-Phase of Formamidinium Lead Iodide by Optical Spectroscopies

Valentina Carpenella, Francesca Ripanti,* Elena Stellino, Claudia Fasolato, Alessandro Nucara, Caterina Petrillo, Lorenzo Malavasi, and Paolo Postorino

Cite This: J. Phys. Chem. C 2023, 127, 2440−2447

Read Online

ACCESS | Metrics & More | Article Recommendations | Supporting Information

ABSTRACT: The exceptional photovoltaic properties of hybrid organic−inorganic perovskites have attracted increasing interest in the past decades. Among these materials, $FAPbI_3$ shows two structural phases: the high temperature perovskite α-phase, with direct bandgap close to the Shockley−Queisser limit, and the much less photoactive non-perovskite δ-phase, stable at ambient conditions. Although the presence of the δ-phase has been usually regarded as a limitation for $FAPbI_3$ optoelectronic applications, recent studies have found that devices with increased stability and efficiency can be designed by mixing α- and δ-phases. This has brought out the need for a deeper understanding of the physical properties of δ-$FAPbI_3$. In this paper, we present an original high-pressure Raman and photoluminescence study to address the effects of compression on the lattice and optoelectronic response of the sample. Also, based on the previous findings on different hybrid perovskites, our results for δ-$FAPbI_3$ show that the cation configuration goes from a dynamically disordered regime at ambient conditions to a statically ordered phase at ∼1.5 GPa. On further increasing pressure, above 7 GPa, a statically disordered regime takes place, where the cations are locked at random orientations in the inorganic framework, giving rise to an amorphous-like state. Compared with α- $FAPbI_3$, we found that the hexagonal δ-phase is less affected by external compression, as both the first detectable structural transition and the amorphous-like behavior occur at higher pressures.

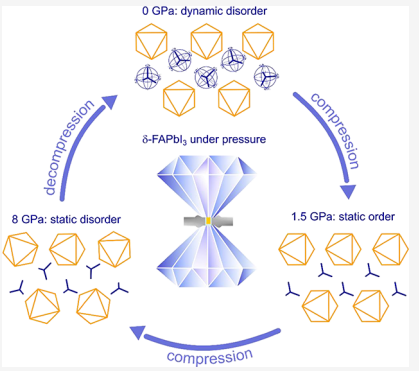

1. INTRODUCTION

Hybrid organic−inorganic perovskites (HOIPs) have attracted enormous attention in the past years as innovative compounds for photovoltaic applications. Because of their low cost, easy fabrication, and extremely promising optoelectronic properties, intense research activities have been devoted to the engineering of highly efficient HOIP-based solar cells, which have reached outstanding power conversion efficiency (PCE) values, as high as 25.7%, in only a couple of decades.[1−3]

The HOIP general formula is ABX_3, where X is a halide anion (I^-, Br^-, or Cl^-), B is a divalent metal atom (Pb^{2+} or Sn^{2+}), and A is an organic cation. The two common organic cations in these compounds are methylammonium ($MA^+ = CH_3NH_3^+$) and formamidinium ($FA^+ = HC(NH_2)_2^+$). In the crystalline configuration, the X and B atoms arrange in an all-inorganic three-dimensional structure of corner-sharing octahedrons, and the organic moiety resides into the interstitial spaces within the inorganic framework. The phase stability of the perovskite structure is determined by the Goldschmidt tolerance factor, defined as $t = (R_A + R_X)/\sqrt{2}(R_B + R_X)$, where R_A, R_B, and R_X are the ionic radii of the ions in the compound. Assuming that the organic molecule is free to rotate around its center of mass, its effective ionic radius R_A can be calculated as discussed by Kieslich et al.,[4] following the relation $R_A = r_{mass} + r_{ion}$ (r_{mass} is the distance between the center of mass and the most distant atom of the molecule, with r_{ion} its corresponding ionic radius). If the calculated tolerance factor t is between 0.9 and 1, the HOIP crystallizes in the cubic structure, while for t outside this range the atoms arrange in a less symmetric configuration.

Among the different HOIP compounds, formamidinium-based systems have emerged in the past few years as the most promising materials for highly efficient photovoltaics.[5,6] Indeed, they show not only an improved long-term stability compared to the methylammonium counterparts but also a smaller bandgap (1.48 eV for cubic $FAPbI_3$[7]), which brings them closer to the Shockley−Queisser limit and extends the light absorption to the near-IR region.

It is known that two different phases of $FAPbI_3$ exist.[8] Because the tolerance factor of $FAPbI_3$ is very close to 1 ($t \sim 0.99$ if one uses the Shannon ionic radii for Pb^{2+} and I^- and the FA^+ radius calculated by Kieslich et al.[4]), at ambient conditions the compound crystallizes in a non-perovskite hexagonal

Received: November 24, 2022
Revised: January 20, 2023
Published: January 27, 2023

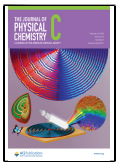

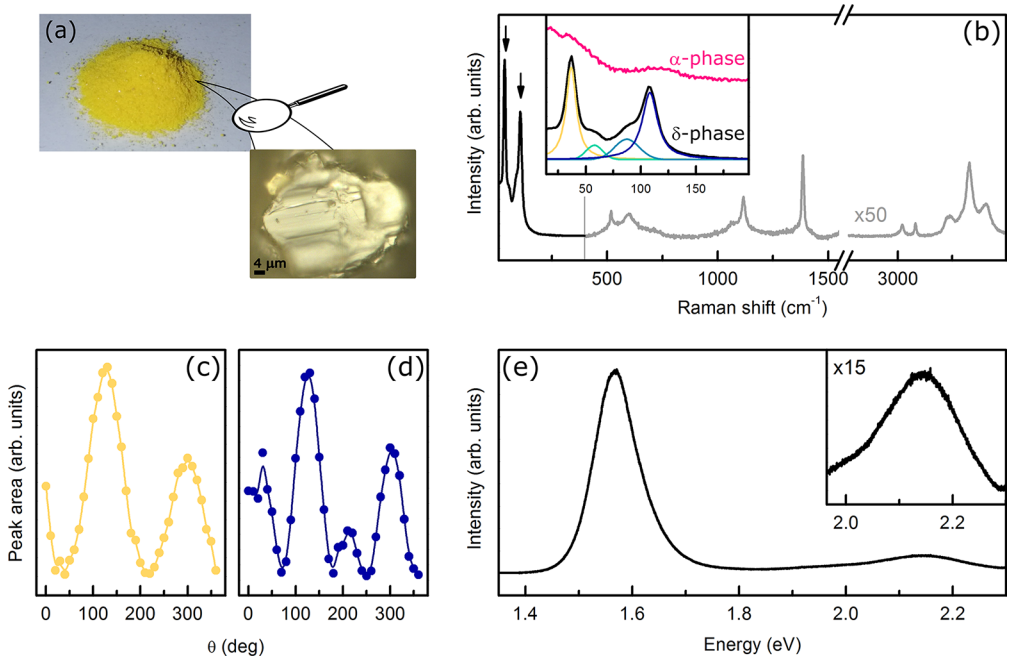

Figure 1. (a) Images of δ-$FAPbI_3$ powder at the millimetric and micrometric scale. (b) Raman spectrum of δ-$FAPbI_3$ sample at ambient pressure collected using 532 nm excitation over the 20−3500 cm^{-1} spectral range. Above 500 cm^{-1} (gray line), the intensity is multiplied by a factor 50, for the sake of clarity. The arrows point to the two most intense peaks analyzed with polarization-dependent Raman measurements. In the inset, comparison between the Raman spectrum of δ-$FAPbI_3$ (black line) and the α-$FAPbI_3$ (pink line) at low wavenumbers. (c, d) Peak area of the most intense Raman active mode at 36 cm^{-1} (yellow) and 108 cm^{-1} (blue) as a function of the polarization angle θ of the incident light. (e) PL signal of the δ-$FAPbI_3$ sample at ambient pressure collected with 532 nm excitation. In the inset, magnification of the spectrum in the 1.9−2.3 eV energy range.

geometry (δ-$FAPbI_3$), yellow in color, in which the neighboring octahedra are organized in a face-sharing arrangement. The α-$FAPbI_3$ perovskite, black in color, with cubic symmetry and corner-sharing octahedra, is achievable by heating δ-$FAPbI_3$ around 150 °C.[8−10] The compound, however, slowly transforms back to the yellow phase with times dependent on the synthesis method.[11−14] The thermally stable δ-$FAPbI_3$ is known for not being photoactive because of its low absorption and larger bandgap (2.14 eV[11]), which implies low efficiency in solar absorption and energy conversion. Moreover, the crystal configuration with face-sharing octahedrons arranged in long chains interferes with electron transport, making δ-$FAPbI_3$ less suitable for photovoltaic applications compared to its cubic counterpart.[12]

Although for decades the δ-phase has been regarded as an undesired product in the synthesis of α-$FAPbI_3$, in the past few years an increasing amount of work has been devoted to the study and the engineering of mixed α/δ phases.[15−20] Zhang et al. reported on the construction of perovskite solar cells made of yellow/black heterophase bilayers, in which a δ-$FAPbI_3$ capping was found to suppress the charge recombination at the interface, enhancing the efficiency and stability of the device.[16] In a similar vein, both Qiu et al.[15] and Giuri et al.[20] were able to realize near-infrared light-emitting diodes exploiting mixed α/δ phases. These new results have brought out the needs for a thorough investigation of the physical properties of δ-$FAPbI_3$, which has been, to date, much less considered with respect to α-$FAPbI_3$.

High-pressure spectroscopy is a powerful tool to explore the structural and electronic properties of HOIPs.[21−23] The study of the crystal response to a reduction in atomic distances provides valuable information about the interacting mechanisms at work in the octahedron cage, inside the molecule, and between the organic and inorganic moieties. Moreover, understanding the system evolution with increasing pressure can be an efficient way to discover new crystalline configurations, with possible improved performances, to be stably synthesized at room temperature through chemical pressure engineering.

In this article, we report on a high-pressure Raman and photoluminescence (PL) investigation of δ-$FAPbI_3$ crystals to study the effects of lattice compression on the lattice dynamics, the optoelectronic properties of the sample, and their possible coupling channels. We observe an increase in the number of Raman-active phonon peaks around 1.5 GPa, indicating a lattice transition to a lower symmetry phase. Then, above 7 GPa, the spectrum line shape turns into a nearly featureless profile, suggesting the occurrence of an amorphization-like process. As to the PL spectrum, the exciton band measured at 2.15 eV, due to the indirect transition of the δ-phase, continuously evolves in the 0−9 GPa pressure range. Combining the results from Raman and PL measurements, we ascribe the transition observed in the Raman spectrum to a distortion of the inorganic framework caused by the pressure induced locking of the organic FA^+ motion at random orientations. This mechanism, previously reported for other HOIPs like $MAPbBr_3$,[24] is here proposed and experimentally supported, for the first time, in a non-perovskite crystal structure.

2. MATERIALS AND METHODS

2.1. Sample Synthesis. The powder δ-$FAPbI_3$ crystals were synthesized from a solution of lead acetate (99.9%) dissolved in an excess of HI in an aqueous solution at 55% by

https://doi.org/10.1021/acs.jpcc.2c08253
J. Phys. Chem. C 2023, 127, 2440−2447

continuous mechanical stirring under a nitrogen atmosphere. The solution is then heated to 100 °C, and the formamidinium amine is thus added (40 wt % in water) in equimolar proportion. The solution is finally cooled at a rate of 1 °C/min until it reaches 46 °C with the formation of a precipitate, which is immediately filtered and dried under vacuum at 60 °C overnight. Formation of the desired δ-$FAPbI_3$ phase was assessed by X-ray diffraction (XRD) analysis using Cu K radiation (Bruker D8 Advance).

2.2. Raman Setup. Raman spectra were collected with a Horiba LabRAM HR Evolution microspectrometer operating in backscattering geometry. The radiation sources employed for the excitation were a 632.8 nm He−Ne laser and a 532 nm solid-state laser, focused on the sample by the use of a microscope equipped with interchangeable objectives with different magnifications (10×, 20×, 50×, and 100×). Experimental spectra were acquired using a 600 grooves/mm diffraction grating and a Peltier-cooled charge-coupled device (CCD) detector. In this configuration, it was possible to reach a spectral resolution better than 3 cm^{-1}. The elastic component of the scattered light was removed by a volume Bragg grating optical filter,[25] which allows for Raman spectra acquisition at Raman shift as low as 10 cm^{-1} from the laser line. The spectra were analyzed using Origin software.

Polarization-dependent Raman spectra were collected using a $\lambda/2$ waveplate placed in the "vertical−vertical" configuration,[26] used to rotate the polarization on the sample surface, and a polarization analyzer. Further details on the polarization measurements can be found in the Supporting Information.

2.3. High-Pressure Setup. For the high-pressure setup, a diamond anvil cell (DAC) with a 400 μm diameter culet was employed to achieve the desired pressure range. A molybdenum gasket of original thickness of 250 μm was indented in between the diamond culet until the final thickness of ∼50 μm was reached. A 150 μm diameter hole was drilled in the center of the indentation and filled with NaCl powder as pressure transmitting medium. Indeed, some trial measurements were previously performed during the preparatory stage, loading the cell with NaCl powder or a liquid mixture 4:1 of methanol and ethanol. In the latter case, the quality of the $FAPbI_3$ microcrystals was reduced by the mixture, as indicated by evident modifications in the low-frequency Raman spectrum of the sample. The cell was then mildly compressed to obtain a NaCl crystalline pellet. The δ-$FAPbI_3$ powdered sample was finally embedded in the NaCl crystal together with a ruby microsphere used as pressure calibrant.[27]

3. RESULTS

3.1. Ambient Pressure Characterization of the δ-$FAPbI_3$ Sample. Powder δ-$FAPbI_3$, with a zoom on a single grain, is shown in Figure 1a. Because of the small area of the incident laser spot (a few μm^2, smaller than the single grain surface), it is possible to perform an accurate investigation of the crystal in a spatially confined area. In the Raman spectrum of δ-$FAPbI_3$, both the inorganic octahedron vibrations, below 200 cm^{-1}, and the formamidinium molecular vibrations, in the frequency range above ∼500 cm^{-1}, can be observed. The complete δ-$FAPbI_3$ Raman spectrum, collected over the 20−3500 cm^{-1} spectral range, is shown in Figure 1b.

A comparative analysis with other studies on FA-based compounds allows for a tentative assignment of the observed vibrational modes, associated with the formamidinium molecular vibrations,[28,29] as reported in Table S2. In the 500−1600 cm^{-1} range, four intense peaks are indeed observed. The spectral feature at 518 cm^{-1} is ascribed to the $H_2N-C-NH_2$ bending mode, while the one at 592 cm^{-1} to the NH_2 wagging. At higher wavenumbers, the peak at 1116 cm^{-1} can be assigned to the C−N stretching vibration and that at 1384 cm^{-1} to the NH_2 rocking mode. The high-frequency features between 3000−3100 cm^{-1} and 3200−3500 cm^{-1} are associated respectively to the C−H and N−H stretching modes.

In the present work, the high-pressure investigation of δ-$FAPbI_3$ is performed focusing on the spectral region below 200 cm^{-1} displaying the vibrational modes of the inorganic cage. Indeed, as samples were loaded in a DAC, we observe an overall reduction of the detected signal, which prevents a clear identification of the low-intensity features above 500 cm^{-1} (see the gray line in Figure 1b, multiplied by a factor 50). Differently from the molecular modes, whose peaks are scarcely affected by cage symmetry changes, the Raman spectrum of the octahedron vibrations below 200 cm^{-1} undergoes significant variations passing from α-$FAPbI_3$ to δ-$FAPbI_3$. As shown in the inset of Figure 1b, the cubic phase, obtained by heating our δ-$FAPbI_3$powder up to ∼200 °C, displays a nearly featureless profile,[13,30] coherent with that expected for $Pm\bar{3}m$ space group of the crystal lattice, while the spectrum of the hexagonal phase is characterized by four distinct peaks at 36, 58, 87, and 108 cm^{-1}.

A reasonable identification of the low-frequency modes of δ-$FAPbI_3$ can be achieved by the comparison with the all-inorganic δ-$CsPbI_3$ phonons. Indeed, in the δ-phase of both FA^+- and Cs-based perovskites, Pb and I atoms arrange in face-sharing octahedrons (although the space group is different in the two cases) and are thus involved in vibrational modes with similar symmetry and energy. On the basis of the assignment proposed by Yang et al. for δ-$CsPbI_3$,[31] we can identify in the δ-$FAPbI_3$ spectrum the phonon peak associated with the equatorial I−Pb−I bending with double octahedral axial stretching at 36 cm^{-1}, that associated with the I−Pb−I bending and stretching with double octahedral distortion at 58 cm^{-1}, that corresponding to the equatorial double octahedral shearing at 87 cm^{-1}, and, finally, the one ascribed to the I−Pb−I stretching with double octahedral expansion at 108 cm^{-1}. A summary of all the observed vibrational modes of the cage is reported in Table S1.

Polarization-dependent Raman measurements were performed in the 15−200 cm^{-1} range to check the crystal quality and to further support the assignment of the peaks. The peak area of the two most intense Raman-active modes (36 and 108 cm^{-1}, indicated by arrows in Figure 1b) as a function of the polarization angle θ of the incident light is shown in Figure 1c,d. Under reasonable assumptions on the crystal orientation (see the Supporting Information), we find that the angle dependence of the peak at 36 cm^{-1} is compatible with that expected for a A_1 total symmetric mode, while the peak at 108 cm^{-1} follows the trend expected for a doubly degenerate E mode, in agreement with the assignment proposed in ref 31. The well-defined periodicity of the two trends is evidence of the good crystal quality of the sample grains and proves that the powder sample is indeed composed of micrometer-sized single crystals.

Figure 1e displays the measured photoluminescence (PL) signal of our sample. At ambient pressure, the spectrum consists of a very intense peak centered at 1.53 eV and of a secondary, smaller peak at 2.15 eV (visible in the enlarged inset

https://doi.org/10.1021/acs.jpcc.2c08253
J. Phys. Chem. C 2023, 127, 2440−2447

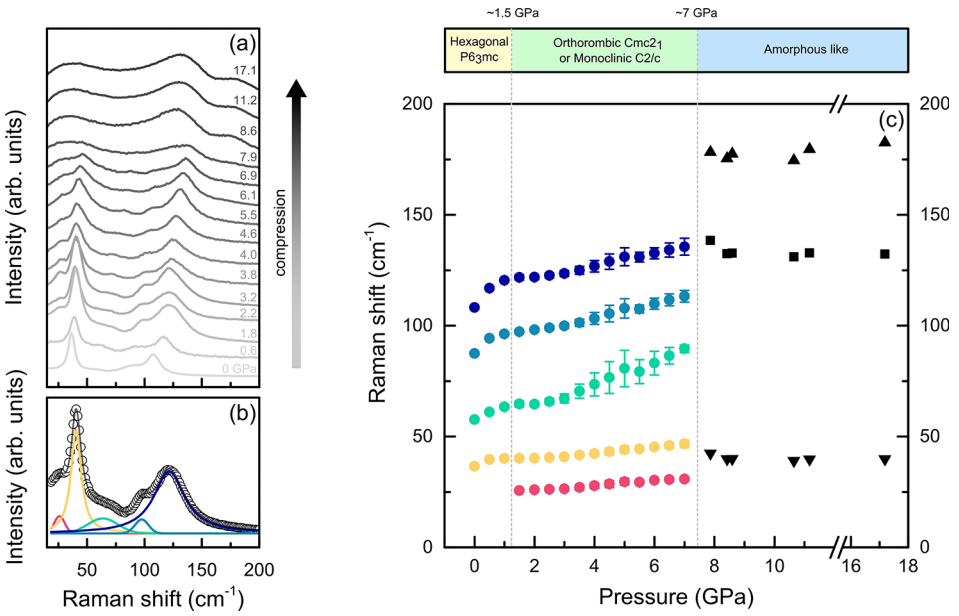

Figure 2. (a) High-pressure δ-$FAPbI_3$ Raman spectra in the 15−200 cm^{-1} range during the compression route. (b) Representative fitting deconvolution of the spectrum at 1.8 GPa. (c) Peak position as a function of pressure during the compression route. The structural phases at different pressures are described in the upper panel, with phase transitions being marked by vertical dashed lines. Data between 0 and 7 GPa were obtained by the average of the different data sets with error bars obtained as standard deviations (for further details see Figure S3). Data above 7 GPa were obtained by fitting each available single spectral profile.

of Figure 1e). The position of the first band is compatible with that expected for the direct exciton of α-$FAPbI_3$,[7,11] while the second band at higher energy can be ascribed to the exciton of the δ-$FAPbI_3$ bandgap.[11] Despite the high intensity of the α-exciton band, the yellow appearance of the sample (Figure 1a) ensures that any α-$FAPbI_3$ domains, although present, represent a minimal percentage of the sample composition. The presence of spurious clusters is commonly reported in HOIP crystals and mostly depends on the synthesis conditions.[8,32] In the present case, α-$FAPbI_3$ domains, embedded in the main phase, might be stabilized at room temperature owing to the local strain induced by the surrounding lattice. It is noteworthy that because most of the sample belongs to the δ-phase, the higher intensity of the direct α-exciton band compared to that of the δ-exciton band clearly indicates that the band at 2.15 eV originates from a recombination process through an indirect bandgap. Indeed, indirect transitions involve a phonon contribution to account for the momentum mismatch and are thus intrinsically less probable than direct recombinations. This result represents, to the best of our knowledge, the first experimental indication of the indirect nature of the bandgap of δ-$FAPbI_3$, previously predicted by *ab initio* calculations.[7]

3.2. High-Pressure Raman Measurements. The high-pressure spectra of δ-$FAPbI_3$ in the low-frequency region are shown in Figure 2a. The sample was compressed up to 17 GPa at room temperature.

As shown in Figure 2a, the spectral profile of δ-$FAPbI_3$ at ambient pressure consists of two intense peaks at 36 and 108 cm^{-1} and two broader shoulders at 58 and 87 cm^{-1}. With increasing pressure, as expected, a general hardening of the whole spectrum is observed. Moreover, at 1.5 GPa a new peak appears in the spectrum at 25 cm^{-1}. At pressures above 7 GPa, the line shape of the spectrum changes from four well-defined peaks to a three-broadband profile, where all the above-mentioned main distinctive features are lost. The new spectral profile can be associated with the transformation toward a new amorphous-like phase[24] and, basically, does not change with further increasing pressure up to 17 GPa.

The peak position as a function of the applied pressure is reported in Figure 2c. A careful inspection of the pressure dependence of the peak positions reveals a change of slope at 1.5 GPa for all the Raman-active modes. Moreover, a new peak at 25 cm^{-1} appears at the same pressure threshold, as displayed in Figure 2b. The combination of these findings suggests that a distortion of the crystalline structure occurred. An experimental XRD investigation from Jiang et al.[33] showed that around 1.7 GPa δ-$FAPbI_3$ goes through a mild lattice distortion that transforms the crystalline symmetry from the hexagonal $P6_3mc$ space group to the orthorhombic $Cmc2_1$, which differs from the former by a slight shift of the octahedron position. Furthermore, different high-pressure XRD measurements and enthalpy calculations performed by Wang et al.[7] revealed a phase transition above 1 GPa to the monoclinic $C2/c$ phase. Even though the final space group of δ-$FAPbI_3$ is still a topic of debate, the pressure evolution of the Raman spectrum in the 0−2 GPa range, characterized by an increase in the number of phonon peaks, confirms the occurrence of a phase transition to a lower symmetry phase.

As previously discussed, the Raman line shape transforms when the applied pressure reaches 7 GPa. The frequency position of the three broad bands is kept constant up to the highest pressure achieved, as shown in Figure 2c.

In order to investigate the reversibility of the transition, Raman spectra were also collected with releasing pressure. As shown in Figure 3a, the line shape of the Raman spectrum does not retrieve its original appearance with decompression. The trend of the peak position, reported in Figure 3b, shows that the three main contributions to the spectrum undergo a mild softening of the peak position down to minimum pressure of 0.7 GPa. Then, as the sample is brought back at ambient conditions, the Raman spectrum recovers its original four-peak

https://doi.org/10.1021/acs.jpcc.2c08253
J. Phys. Chem. C 2023, 127, 2440−2447

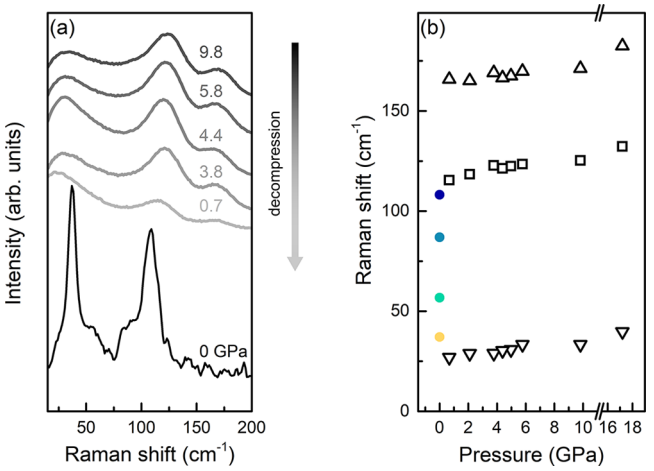

Figure 3. (a) Low-frequency δ-$FAPbI_3$ Raman spectra during the decompression route (in grayscale) and at ambient conditions (black line). (b) Analysis of the peak position during the decompression route. The black empty symbols are the band positions at $P > 0$ GPa, while the colored dots are the peak positions observed at ambient conditions after the pressure is released.

profile although with an overall intensity reduction with respect to the pristine ambient condition spectrum due to the increased lattice disorder. The peak centers, reported in Figure 3b, coincide with those measured before the compression−decompression route.

Previous studies on α-FAPI have shown that the crystal undergoes two structural distortions at ∼0.3 and ∼1.7 GPa, followed by a transition to an amorphous-like phase at ∼4 GPa.[7,29] The present results thus show that the hexagonal δ-phase of $FAPbI_3$ is less affected by external compression, as both the first detectable structural transition and the amorphous-like behavior occur at higher pressures.

3.3. High-Pressure Photoluminescence Measurements. Parallel to the Raman investigation, aimed at assessing the high-pressure behavior of the vibrational modes of δ-$FAPbI_3$, its electronic properties were also studied as a function of pressure. The spectra obtained from the high-pressure PL experiments are reported in Figure 4 for both the compression and the decompression route.

As reported in the inset of Figure 4a, the α-exciton band, above ascribed to the presence of α-$FAPbI_3$ clusters (see Section 3.1), shifts from 1.53 to 1.47 eV in the 0−1.4 GPa range and vanishes at 2.8 GPa. This is in agreement with previous studies on pristine α-$FAPbI_3$, where a similar red-shift followed by an abrupt quenching of the PL emission at about 3.5 GPa was observed.[7] The authors ascribed this effect to an enhancement in non-radiative processes due to a progressive amorphization of the lattice. The lower pressure threshold (2.8 GPa vs 3.5 GPa) found in our case can be due to the effect of strain experienced by the α domains when embedded in the δ-$FAPbI_3$ lattice. During decompression (see the inset in Figure 4b), as pressure reaches 1.9 GPa, the α-exciton band is restored in agreement with previous results from the literature.[7]

As to δ-$FAPbI_3$, the indirect exciton band at 2.15 eV (see Section 3.1) vanishes at the first working pressure (1.4 GPa), as reported in Figure 4a. Then, at 2.8 GPa, in correspondence with the suppression of the exciton of α-$FAPbI_3$, a broad band appears at 1.9 eV and remains almost fixed on further increasing pressure. Notice that between 0 and 2 GPa, the indirect exciton band of δ-$FAPbI_3$ is superimposed to the high-

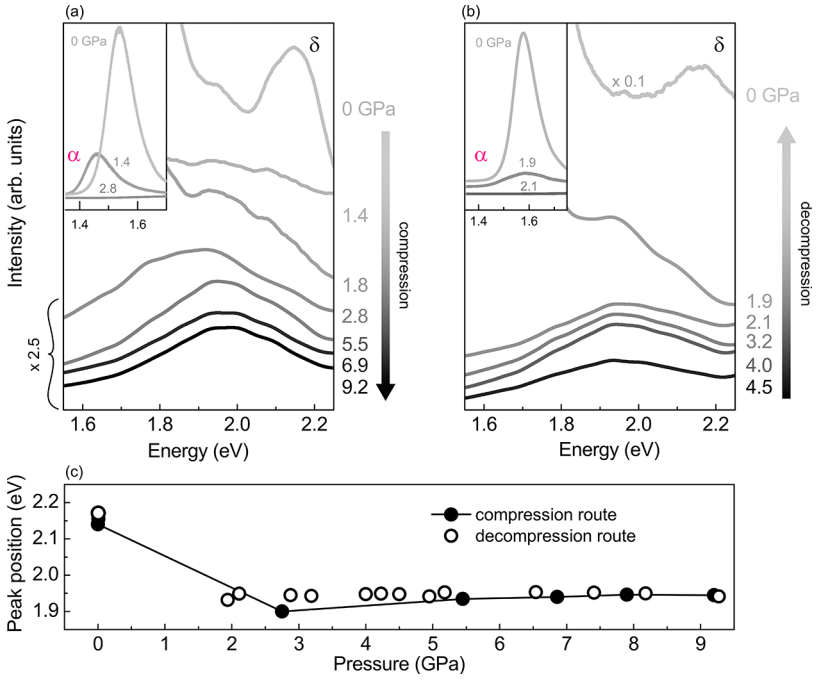

Figure 4. δ-$FAPbI_3$ PL spectra (vertically shifted for sake of clarity) collected on (a) increasing and (b) decreasing pressure in the 1.6−2.2 eV range. All the spectra were normalized to the same acquisition time and subjected to a smoothing procedure. The narrow peaks ascribed to diamond vibrational modes (at ∼2.16 eV) and ruby fluorescence emission (at ∼1.78 eV) were subtracted to the data. Some of the spectra were also multiplied by a constant factor, as shown in the figures, for sake of clarity. The insets show the pressure evolution of the exciton band corresponding to the α-$FAPbI_3$ direct bandgap. (c) Peak position of the δ-$FAPbI_3$ PL spectra during compression (full spheres) and decompression (empty circles).

https://doi.org/10.1021/acs.jpcc.2c08253
J. Phys. Chem. C 2023, 127, 2440−2447

energy tail of the direct exciton band of the α-phase clusters and is thus less visible. The quenching of the indirect δ-exciton at 1.4 GPa can be explained with the increase in non-radiative recombination processes due to the pressure-induced increase in lattice disorder. It is worth noticing that this effect is observed also in the PL band of α-$FAPbI_3$, whose spectral weight is significantly reduced with pressure. However, in this case, the higher intensity of the signal and the direct nature of the transition allows us to detect the band also on applying pressure. When the direct exciton of α-$FAPbI_3$ is suppressed at 2.8 GPa, the indirect exciton of the δ-$FAPbI_3$ is left as the only possible radiative decay channel and becomes visible again in the spectrum. The 0.25 eV red-shift observed in the indirect exciton center (Figure 4c) is compatible with a pressure-induced reduction of the indirect gap of δ-$FAPbI_3$ in the 0−2.8 GPa range.

During the decompression route, shown in Figure 4b, the δ-exciton band keeps its center at about 1.9 eV between 9 and 2 GPa. Below 2 GPa, as the direct decay channel becomes available again, the intensity of the indirect band is strongly quenched. Finally, once the sample is brought back at ambient conditions, the δ-exciton turns visible again, centered at its original energy (~2.15 eV).

4. DISCUSSION

Combining the results from Raman and PL measurements, we can draw a coherent scenario for the pressure evolution of δ-$FAPbI_3$, in analogy to that proposed in the literature for similar compounds.[24,34]

At ambient conditions, the crystal exhibits a dynamically disordered structure, in which the organic cation is rotationally averaged over equivalent orientations, and thus, the long-range periodicity is governed mainly by the inorganic framework.[35] The application of pressure drives the shortening of the H−I bonds, which progressively inhibits the rotation of FA^+ cations. We propose that at 1.5 GPa, similarly to that observed for MA-based perovskites by Capitani et al.[24] and by Francisco-Lopez et al.[36] at increasing pressure and by Leguy et al.[37] and Sharma et al.[38] at decreasing temperature, a statically ordered regime sets up, in which the orientation of the cations shows a periodic arrangement. In this configuration, the inorganic framework takes a lower-symmetry phase, and new peaks appear in the Raman spectrum of the sample, as discussed in Section 3.2. On further increasing pressure above 7 GPa, a statically disordered regime takes place, in which the FA^+ cations are locked at random orientations. Correspondingly, the octahedral chains undergo local distortions making the crystal lose its long-range periodicity. As a result, all Raman-active features broaden giving rise to an amorphous-like spectrum. We believe that, in this high-pressure state, although the lack of long-range order strongly damps the vibrational modes, the sample maintains locally an octahedral symmetry in the inorganic framework. This idea is supported by the reversibility of the Raman spectrum when the sample is brought back to ambient conditions, which could not occur in the case of a complete deconstruction of the inorganic framework.

Whereas an abrupt discontinuity of the evolution of the Raman spectrum on increasing the pressure from 6 to 8 GPa is observed, the PL band does not change over the same pressure range. Raman and PL responses are expected to be at least partially coupled, since the vibrational modes below 200 cm^{-1} involve the Pb and I atoms, whose orbitals are those mainly contributing to the valence and conduction bands of the crystal.[7] The absence of appreciable modifications of the PL spectrum provides further support to the idea that the Pb−I bonds within the inorganic framework maintains the local octahedral structure and that the insurgence of a statically disordered regime, signaled by Raman, is driven by the random orientation of FA^+.

5. CONCLUSIONS

To sum up, high-pressure Raman and PL measurements allowed us to shed light on the fundamental role played by the interaction between organic and inorganic moiety in the lattice dynamics and the optoelectronic response of δ-$FAPbI_3$. In particular, we found that the pressure evolution of this sample shares strong similarities with that previously observed for crystals in a properly perovskite form. Bearing in mind the hexagonal symmetry of the δ-phase, this suggests that the driving force of the amorphous-like molecular disorder is octahedral compression. Our results contribute to reaching a deeper understanding of the physical properties of a compound that has been scarcely studied in the literature due to its non-perovskite structure but that has recently demonstrated to play a key role in the performance of devices exploiting mixed α/δ phases.

■ ASSOCIATED CONTENT

Supporting Information

The Supporting Information is available free of charge at https://pubs.acs.org/doi/10.1021/acs.jpcc.2c08253.

Further details on the analysis on the Raman spectrum of δ-$FAPbI_3$ at room and high pressure, together with the polarization-dependent Raman measurements (PDF)

■ AUTHOR INFORMATION

Corresponding Author

Francesca Ripanti − *Department of Physics and Geology, University of Perugia, 06123 Perugia, Italy;* orcid.org/0000-0002-9505-740X; Email: francesca.ripanti@unipg.it

Authors

Valentina Carpenella − *Department of Sciences, University of Roma Tre, 00146 Rome, Italy;* orcid.org/0000-0002-0631-8189

Elena Stellino − *Department of Physics and Geology, University of Perugia, 06123 Perugia, Italy;* orcid.org/0000-0001-6385-4589

Claudia Fasolato − *CNR-ISC, Istituto dei Sistemi Complessi, c/o Sapienza University of Rome, 00185 Rome, Italy;* orcid.org/0000-0003-3450-404X

Alessandro Nucara − *CNR-SPIN and Department of Physics, Sapienza University of Rome, 00185 Rome, Italy*

Caterina Petrillo − *Department of Physics and Geology, University of Perugia, 06123 Perugia, Italy*

Lorenzo Malavasi − *Department of Chemistry and INSTM, University of Pavia, 27100 Pavia, Italy;* orcid.org/0000-0003-4724-2376

Paolo Postorino − *Department of Physics, Sapienza University of Rome, 00185 Rome, Italy;* orcid.org/0000-0002-3809-0676

Complete contact information is available at: https://pubs.acs.org/10.1021/acs.jpcc.2c08253

Author Contributions

V.C., F.R., and E.S. performed the measurements. V.C. performed the data analysis and wrote the draft with the contribution of F.R. and E.S. L.M. synthesized the sample. C.F., A.N., and C.P. contributed to the interpretation of the results and critically reviewed the paper. P.P. conceived and supervised the work. All the authors discussed the results and revised the article.

Notes

The authors declare no competing financial interest.

■ ACKNOWLEDGMENTS

This research work was supported by the CarESS project, D.R. no. 597, from the University of Perugia.

■ REFERENCES

(1) Best Research-Cell Efficiency Chart, https://www.nrel.gov/pv/cell-efficiency.html.
(2) Kim, J. Y.; Lee, J. W.; Jung, H. S.; Shin, H.; Park, N. G. High-efficiency perovskite solar cells. *Chem. Rev.* **2020**, *120* (15), 7867−7918.
(3) Li, X.; Bi, D.; Yi, C.; Décoppet, J. D.; Luo, J.; Zakeeruddin, S. M.; Hagfeldt, A.; Grätzel, M. A vacuum flash−assisted solution process for high-efficiency large-area perovskite solar cells. *Science* **2016**, *353* (6294), 58−62.
(4) Kieslich, G.; Sun, S.; Cheetham, A. K. Solid-state principles applied to organic−inorganic perovskites: new tricks for an old dog. *Chem. Sci.* **2014**, *5* (12), 4712−4715.
(5) Min, H.; Kim, M.; Lee, S. U.; Kim, H.; Kim, G.; Choi, K.; Lee, J. H.; Seok, S. I. Efficient, stable solar cells by using inherent bandgap of α-phase formamidinium lead iodide. *Science* **2019**, *366* (6466), 749−753.
(6) Zhao, Y.; Tan, H.; Yuan, H.; Yang, Z.; Fan, J. Z.; Kim, J.; Voznyy, O.; Gong, X.; Quan, L. N.; Tan, C. S.; et al. Perovskite seeding growth of formamidinium-lead-iodide-based perovskites for efficient and stable solar cells. *Nat. Commun.* **2018**, *9* (1), 1−10.
(7) Wang, P.; Guan, J.; Galeschuk, D. T.; Yao, Y.; He, C. F.; Jiang, S.; Zhang, S.; Liu, Y.; Jin, M.; Jin, C.; et al. Pressure-induced polymorphic, optical, and electronic transitions of formamidinium lead iodide perovskite. *J. Phys. Chem. Lett.* **2017**, *8* (10), 2119−2125.
(8) Stoumpos, C. C.; Malliakas, C. D.; Kanatzidis, M. G. Semiconducting tin and lead iodide perovskites with organic cations: phase transitions, high mobilities, and near-infrared photoluminescent properties. *Inorg. Chem.* **2013**, *52* (15), 9019−9038.
(9) Lee, J. W.; Kim, D. H.; Kim, H. S.; Seo, S. W.; Cho, S. M.; Park, N. G. Formamidinium and cesium hybridization for photo-and moisture-stable perovskite solar cell. *Adv. Energy Mater.* **2015**, *5* (20), 1501310.
(10) Jeon, N. J.; Noh, J. H.; Yang, W. S.; Kim, Y. C.; Ryu, S.; Seo, J.; Seok, S. I. Compositional engineering of perovskite materials for high-performance solar cells. *Nature* **2015**, *517* (7535), 476−480.
(11) Han, Q.; Bae, S. H.; Sun, P.; Hsieh, Y. T.; Yang, Y.; Rim, Y. S.; Zhao, H.; Chen, Q.; Shi, W.; Li, G.; et al. Single crystal formamidinium lead iodide ($FAPbI_3$): insight into the structural, optical, and electrical properties. *Adv. Mater.* **2016**, *28* (11), 2253−2258.
(12) Koh, T. M.; Fu, K.; Fang, Y.; Chen, S.; Sum, T. C.; Mathews, N.; Mhaisalkar, S. G.; Boix, P. P.; Baikie, T. Formamidinium-containing metal-halide: an alternative material for near-IR absorption perovskite solar cells. *J. Phys. Chem. C* **2014**, *118* (30), 16458−16462.
(13) Driscoll, E. H.; Orera, A.; Anderson, P. A.; Sanjuan, M. L.; Slater, P. R. Raman spectroscopy insights into the α-and δ-phases of formamidinium lead iodide ($FAPbI_3$). *Dalton Trans* **2021**, *50* (9), 3315−3323.
(14) He, W.; Hu, J.; Chen, C.; Chen, Y.; Zeng, L.; Zhang, X.; Cai, B.; Mai, Y.; Guo, F. Temperature-Assisted Crystal Growth of Photovoltaic α-Phase $FAPbI_3$ Thin Films by Sequential Blade Coating. *ACS Appl. Mater. Interfaces* **2020**, *12* (50), 55830−55837.
(15) Qiu, J.; Tang, L.; Xia, Y.; Guo, J.; Xing, G.; Wang, F.; Dong, Q.; Chen, Y.; Huang, W. Stable, efficient near-infrared light-emitting diodes enabled by α/δ phase modulation. *J. Phys. Chem. Lett.* **2019**, *10* (9), 2101−2107.
(16) Zhang, J.; Jiang, X.; Liu, X.; Guo, X.; Li, C. Maximizing Merits of Undesirable δ-FAPbI3 by Constructing yellow/black Heterophase Bilayer for Efficient and Stable Perovskite Photovoltaics. *Adv. Funct. Mater.* **2022**, *32* (44), 2204642.
(17) Giuri, A.; Munir, R.; Listorti, A.; Corcione, C. E.; Gigli, G.; Rizzo, A.; Amassian, A.; Colella, S. Implication of polymeric template agent on the formation process of hybrid halide perovskite films. *Nanotechnology* **2021**, *32* (26), 265707.
(18) Lee, Y. M.; Yun, J. H.; Matsuyama, A.; Kobori, S.; Maeng, I.; Lyu, M.; Wang, S.; Wang, L.; Jung, M. C.; Nakamura, M. Significant THz-wave absorption property in mixed δ-and α-$FAPbI_3$ hybrid perovskite flexible thin film formed by sequential vacuum evaporation. *Appl. Phys. Express* **2019**, *12* (5), 051003.
(19) Maeng, I.; Lee, S.; Han, E. Q.; Zhang, Y.; Oh, S. J.; Nakamura, M.; Yun, J. H.; Wang, L.; Kwon, Y. K.; Jung, M. C. Unusual terahertz-wave absorptions in δ/α-mixed-phase $FAPbI_3$ single crystals: interfacial phonon vibration modes. *NPG Asia Mater.* **2021**, *13* (1), 1−8.
(20) Giuri, A.; Yuan, Z.; Miao, Y.; Wang, J.; Gao, F.; Sestu, N.; Saba, M.; Bongiovanni, G.; Colella, S.; Esposito Corcione, C.; et al. Ultra-bright near-infrared perovskite light-emitting diodes with reduced efficiency roll-off. *Sci. Rep* **2018**, *8* (1), 1−8.
(21) Coduri, M.; Strobel, T. A.; Szafrański, M.; Katrusiak, A.; Mahata, A.; Cova, F.; Bonomi, S.; Mosconi, E.; De Angelis, F.; Malavasi, L. Band gap engineering in $MASnBr_3$ and $CsSnBr_3$ perovskites: mechanistic insights through the application of pressure. *J. Phys. Chem. Lett.* **2019**, *10* (23), 7398−7405.
(22) Jaffe, A.; Lin, Y.; Beavers, C. M.; Voss, J.; Mao, W. L.; Karunadasa, H. I. High-pressure single-crystal structures of 3D lead-halide hybrid perovskites and pressure effects on their electronic and optical properties. *ACS Cen. Sci.* **2016**, *2* (4), 201−209.
(23) Postorino, P.; Malavasi, L. Pressure-induced effects in organic−inorganic hybrid perovskites. *J. Phys. Chem. Lett.* **2017**, *8* (12), 2613−2622.
(24) Capitani, F.; Marini, C.; Caramazza, S.; Dore, P.; Pisanu, A.; Malavasi, L.; Nataf, L.; Baudelet, F.; Brubach, J. B.; Roy, P.; et al. Locking of methylammonium by pressure-enhanced H-bonding in $(CH_3NH_3)PbBr_3$ hybrid perovskite. *J. Phys. Chem. C* **2017**, *121* (50), 28125−28131.
(25) Glebov, A. L.; Mokhun, O.; Rapaport, A.; Vergnole, S.; Smirnov, V.; Glebov, L. B. Volume Bragg gratings as ultra-narrow and multiband optical filters. *Micro-Optics* **2012**, *8428*, 42−52.
(26) Ripanti, F.; D'Acunto, G.; Betti, M. G.; Mariani, C.; Bittencourt, C.; Postorino, P. Polarization effects of transversal and longitudinal optical phonons in bundles of multiwall carbon nanotubes. *J. Phys. Chem. C* **2019**, *123* (32), 20013−20019.
(27) Barnett, J. D.; Block, S.; Piermarini, G. J. An optical fluorescence system for quantitative pressure measurement in the diamond-anvil cell. *Rev. Sci. Instrum.* **1973**, *44* (1), 1−9.
(28) Ruan, S.; McMeekin, D. P.; Fan, R.; Webster, N. A.; Ebendorff-Heidepriem, H.; Cheng, Y. B.; Lu, J.; Ruan, Y.; McNeill, C. R. Raman spectroscopy of formamidinium-based lead halide perovskite single crystals. *J. Phys. Chem. C* **2020**, *124* (4), 2265−2272.
(29) Wang, L.; Wang, K.; Zou, B. Pressure-induced structural and optical properties of organometal halide perovskite-based formamidinium lead bromide. *J. Phys. Chem. Lett.* **2016**, *7* (13), 2556−2562.
(30) Sacchetti, A.; Baldini, M.; Postorino, P.; Martin, C.; Maignan, A. Raman spectroscopy on cubic and hexagonal $SrMnO_3$. *J. Raman Spectrosc.* **2006**, *37* (5), 591−596.
(31) Yang, Y.; Robbins, J. P.; Ezeonu, L.; Ma, Y.; Sparta, N.; Kong, X.; Strauf, S.; Podkolzin, S. G.; Lee, S. S. Probing lattice vibrations of stabilized $CsPbI_3$ polymorphs via low-frequency Raman spectroscopy. *J. Mater. Chem. C* **2020**, *8* (26), 8896−8903.

https://doi.org/10.1021/acs.jpcc.2c08253
J. Phys. Chem. C 2023, 127, 2440−2447

(32) Weber, O. J.; Ghosh, D.; Gaines, S.; Henry, P. F.; Walker, A. B.; Islam, M. S.; Weller, M. T. Phase behavior and polymorphism of formamidinium lead iodide. *Chem. Mater.* **2018**, *30* (11), 3768−3778.
(33) Jiang, S.; Luan, Y.; Jang, J. I.; Baikie, T.; Huang, X.; Li, R.; Saouma, F. O.; Wang, Z.; White, T. J.; Fang, J. Phase transitions of formamidinium lead iodide perovskite under pressure. *J. Am. Chem. Soc.* **2018**, *140* (42), 13952−13957.
(34) Capitani, F.; Marini, C.; Caramazza, S.; Postorino, P.; Garbarino, G.; Hanfland, M.; Pisanu, A.; Quadrelli, P.; Malavasi, L. High-pressure behavior of methylammonium lead iodide ($MAPbI_3$) hybrid perovskite. *J. Appl. Phys.* **2016**, *119* (18), 185901.
(35) Szafranski, M.; Katrusiak, A. Mechanism of pressure-induced phase transitions, amorphization, and absorption-edge shift in photovoltaic methylammonium lead iodide. *J. Phys. Chem. Lett.* **2016**, *7* (17), 3458−3466.
(36) Francisco-López, A.; Charles, B.; Weber, O. J.; Alonso, M. I.; Garriga, M.; Campoy-Quiles, M.; Weller, M. T.; Goñi, A. R. Pressure-induced locking of methylammonium cations versus amorphization in hybrid lead iodide perovskites. *J. Phys. Chem. C* **2018**, *122* (38), 22073−22082.
(37) Leguy, A. M.; Goñi, A. R.; Frost, J. M.; Skelton, J.; Brivio, F.; Rodríguez-Martínez, X.; Weber, O. J.; Pallipurath, A.; Alonso, M. I.; Campoy-Quiles, M.; et al. Dynamic disorder, phonon lifetimes, and the assignment of modes to the vibrational spectra of methylammonium lead halide perovskites. *Phys. Chem. Chem. Phys.* **2016**, *18* (39), 27051−27066.
(38) Sharma, R.; Dai, Z.; Gao, L.; Brenner, T. M.; Yadgarov, L.; Zhang, J.; Rakita, Y.; Korobko, R.; Rappe, A. M.; Yaffe, O. Elucidating the atomistic origin of anharmonicity in tetragonal $CH_3NH_3PbI_3$ with Raman scattering. *Phys. Rev. Mater.* **2020**, *4* (9), 092401.

https://doi.org/10.1021/acs.jpcc.2c08253
J. Phys. Chem. C 2023, 127, 2440−2447